Facile Synthesis of Co−B Amorphous Alloy in Uniform Spherical Nanoparticles with Enhanced Catalytic Properties

Zhonghong Zhu, Jinqiang Ma, Liang Xu, Lei Xu, Hexing Li, and Hui Li*

The Education Ministry Key Lab of Resource Chemistry and Shanghai Key Laboratory of Rare Earth Functional Materials, Shanghai Normal University, Shanghai 200234, People's Republic of China

S *Supporting Information*

ABSTRACT: Control of the size and morphology of metallic nanomaterials enables mastery of their properties to enhance their catalytic performances. In this work, uniform Co−B amorphous alloy nanoparticles were synthesized by a simple chemical reduction of $[CoX_4]^-$ with BH_4^- in the presence of Bu_4P^+. With the characterization of X-ray diffraction, selective area electronic diffraction, X-ray photoelectron spectroscopy, differential scanning calorimetry, and transmission electron microscopy, the resulting Co−B spherical nanoparticles were identified to be amorphous alloys in an average particle size around 55 nm. The synergistic effect of the halide anion and Bu_4P^+ cation is essential for the formation of monodisperse and uniform spherical nanoparticles. During the Heck-type carbon−carbon coupling reactions and the hydrogenation of butyraldehyde to *n*-butanol, the as-synthesized Co−B catalyst was extremely active compared with the conventional Co−B obtained via the direct reduction of cobalt ions with BH_4^- in aqueous solution. In addition, the as-prepared Co−B amorphous alloy also exhibited recyclability during the hydrogenation of butyraldehyde due to better thermal stability, which was related to the higher surface B content and the uniform particle size.

KEYWORDS: *Co−B, amorphous alloy, Heck reaction, hydrogenation, high stability*
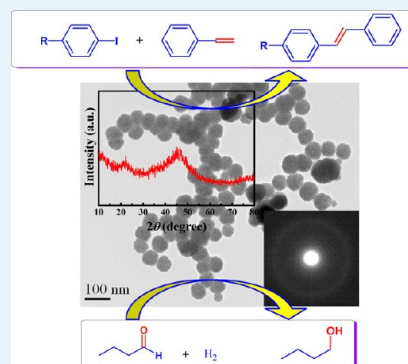
INTRODUCTION

Amorphous alloys, a kind of metastable materials with long-range disordered but short-range ordered structure, have attracted growing attention from both academia and industry because of their superior corrosion resistance, high mechanical toughness, and excellent magnetic, electronic, and catalytic properties in comparison with their crystalline counterparts.[1−4] As heterogeneous catalysts, amorphous alloys have been widely studied because of their excellent catalytic performances.[1−7] To form and stabilize the amorphous structure, some metalloids (e.g., B or P) should be incorporated in amorphous alloys, thus significantly affecting their physical and chemical properties.[8,9] Chemical reduction of metallic ions with borohydride (BH_4^-) in aqueous solution has been most often used to synthesize the kind of M−B amorphous alloy catalysts,[8,9] but vigorous and exothermic reactions between metallic ions and BH_4^- usually induce particle aggregation, thereby reducing catalytic activity. In addition, the nonuniform nanoparticles are also responsible for the ready crystallization of amorphous alloys.[10] Although size-control synthesis of M−B (M = Ni, Co) amorphous alloys could been achieved through microemulsions,[11,12] using large amounts of organic phase in these systems may cause several environmental problem in the preparation process. Recently, we successfully developed a facile method to prepare uniform M−B (M = Ni, Co) amorphous alloy nanoparticles using $[M(NH_3)_6]^{2+}$ as the metal source,[10,13] but the strong coordination of NH_3 to metallic ions and, thus, the very slow

reduction process resulted in relatively large M−B particles (>100 nm) unfavorable for catalytic activity.

The coordination of halide ligands to metallic ions is a well-addressed issue,[14−17] and the interaction between halide and metallic ions is weaker than that between NH_3 and metallic ions. Herein, we report the synthesis of uniform Co−B amorphous alloy nanoparticles through chemical reduction of $[CoX_4]^-$ with BH_4^- in the presence of Bu_4P^+. The catalytic activity of the as-prepared Co−B amorphous alloy was evaluated in the Heck-type carbon−carbon coupling reactions and the hydrogenation of butyraldehyde to *n*-butanol, evidencing enhanced catalytic activity than the Co−B prepared by direct reduction of Co^{2+} with BH_4^-. Moreover, the as-prepared Co−B amorphous alloy also exhibited recyclability during the hydrogenation of butyraldehyde. The correlation of the catalytic performances to the structural properties has been tentatively established.

EXPERIMENTAL PROCEDURES

Catalyst Preparation. All chemicals used in this experiment were analytical grade and were used without further purification. In a typical run of catalyst synthesis, an aqueous solution of $CoCl_2$ (51 mL, 0.10 M) was first added into an aqueous solution of Bu_4PBr (510 mL, 0.050 M), then 210 g of

KCl was added to the above solution to form a saturated solution. Thereafter, an aqueous solution of KBH_4 (40 mL, 0.50 M) was added dropwise under vigorous stirring at 273 K. After the reaction was complete, the black precipitate was washed free from Cl^-, Br^-, or K^+ ions with deionized water until pH ∼ 7 was achieved, followed by three washings with absolute alcohol (EtOH). Finally, the sample was stored in EtOH until use. The as-prepared Co−B sample was designated Co−B−X, with X representing the metal source was Co^{2+} halide ligand complexes. For comparison, a conventional Co−B sample was also prepared by the regular method, that is, by direct reduction of Co^{2+} with BH_4^-,[17] which was designated Co−B−C.

Catalyst Characterization. The bulk composition was analyzed by means of inductively coupled plasma optical emission (ICP; Varian VISTA-MPX). The surface morphology and the particle size were observed by transmission electron micrography (TEM, JEOL JEM-2100). The size distribution was evaluated from about 300 randomly selected particles. The amorphous structure was determined by both X-ray diffraction (XRD; Rigaku D/Max-RB with Cu Kα radiation) and elective area electronic diffraction (SAED; JEOL JEM-2100). The surface electronic states were investigated by X-ray photo-electron spectroscopy (XPS; ULVAC-PHI PHI5000 VersaP-robe using Al Kα radiation), during which all Co−B samples were dried and pretreated in situ in a pure Ar atmosphere to avoid oxidation. The binding energy (BE) values were calibrated by using C 1s = 284.6 eV as a reference. The active surface area (S_{Co}) was measured by hydrogen chemisorption on a Micromeritics AutoChem II 2920 system assuming H/Co(s) = 1 and a surface area of 6.5×10^{-20} m^2 per Co atom.[18] NMR (^{1}H and ^{13}C NMR) spectra were obtained on a Bruker AV-400 NMR spectrometer.

Activity Test. Heck-type Carbon−Carbon Coupling Reactions. In a typical experiment, aryl iodide (5.0 mmol) and terminal alkene (6.0 mmol) were added into 10 mL of mixed solution (DMF/water = 1/1). To this were added catalyst (containing 5.9 mg Co) and K_2CO_3 (7.5 mmol). To avoid the oxidation of the Co−B nanoparticles, high-purity Ar was bubbled through the reaction mixture, and the mixture was stirred at 393 K under argon. Reaction samples were taken at regular intervals and monitored by GC/MS (Agilent 6890n-5973i equipped with a DB-5 capillary column). After the complete reaction, the catalyst was recovered by centrifugation and then washed thoroughly with ether (3 × 3 mL). The solutions were combined and extracted with ether (3 × 3 mL), and analyzed by GC/MS to obtain conversion of aryl halide and selectivity to diphenyl ethylene.

Hydrogenation of Butyraldehyde to *n*-Butanol. Liquid-phase hydrogenation of butyraldehyde was carried out in a 200-mL stainless autoclave containing a catalyst with 0.30 g Co, 4 mL of butyraldehyde, 45 mL of EtOH, and 1.0 MPa of H_2 at 373 K. The reaction system was stirred vigorously (800 rpm) to eliminate the diffusion effects. During the reaction, samples were withdrawn from the reaction mixture at intervals for product analysis on a gas chromatograph equipped with a flame ionization detector and an EC-WAX capillary column. All results have been reproduced, and the errors were limited within ±5%. For the recycling study, the recovered catalyst was further washed sufficiently with ethanol and water.

■ RESULTS AND DISCUSSION

Structural and Electronic Characteristics. The TEM image (Figure 1) reveals that Co−B−C displayed irregular,
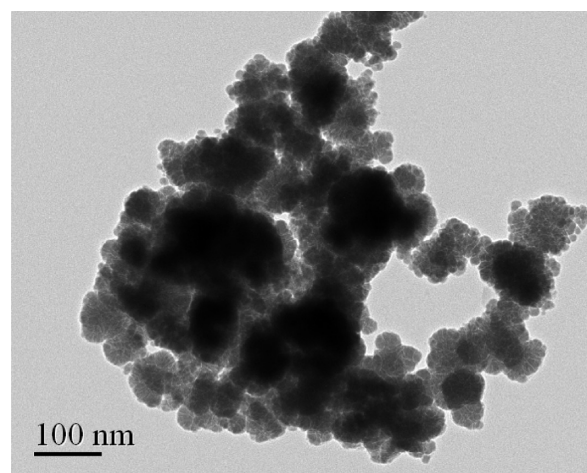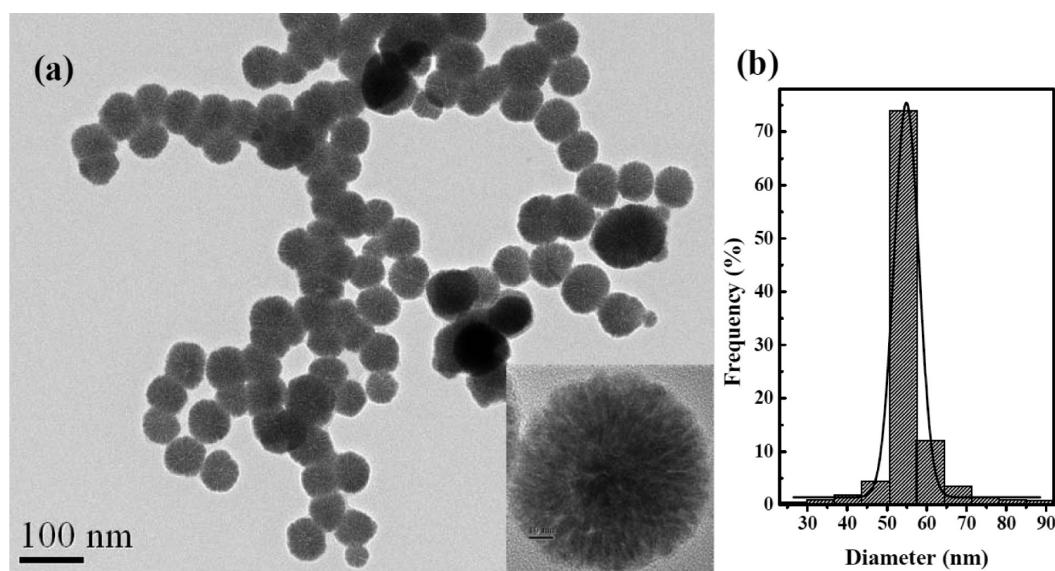

Figure 1. TEM image of Co−B−C.

broadly dispersed particles, from <5 nm to >300 nm. The presence of the large particle is apparently due to the particle agglomeration because the reaction between Co^{2+} and BH_4^- is strongly exothermic.[8] In contrast, the Co−B−X sample synthesized through the present method was monodisperse and with uniformly spherical nanoparticles with an average particle size around 55 nm (Figure 2). From the high-magnification TEM image of a single Co−B−X nanosphere in Figure 2a, the crack structure of Co−B−X with channels radiating from the center could be clearly observed. The relatively narrower distribution for the as-prepared nano-particles could be attributed mainly to both the coordination of X^- (X^- = Cl^- or Br^-) to Co^{2+} and the stabilizing effect of Bu_4P^+. ICP analysis revealed that the B content in Co−B−X was higher than that in Co−B−C (Table 1). This was also due to the smooth reduction induced by the chelating of X^- to Co^{2+}, which could efficiently inhibit the hydrolysis of BH_4^- and, thus, enhance the acidity of the reaction solution and the formation of B-enriched samples.[19] As shown in Table 1, the Co−B−X sample exhibited a much higher S_{Co} than Co−B−C, obviously owing to the absence of the large particles arising from the particle agglomeration.

The XRD patterns presented in Figure 3 show that both the Co−B−C and the Co−B−X synthesized via the present method were present in a typical amorphous alloy structure because only one broad peak centered at $2\theta = 44°$ was observed,[17] as demonstrated by Yokoyama et al.[20] The amorphous alloy structure can be further confirmed by a successive diffraction halo in an attached SAED image.[21] Heat treatment of the fresh Co−B−X sample (at 673 K in N_2 for 2 h) resulted in the appearance of several diffraction peaks corresponding to metallic Co and the crystalline Co−B alloy (Figure 3c). The appearance of Co−B crystalline phases during the crystallization process verified the formation of an alloy between Co and B for the as-prepared Co−B. We infer that except for the crystallization, partial decomposition of a Co−B amorphous alloy may occur in this process.

The crystallization process was further investigated by DSC analysis. As shown in Figure 4a, the Co−B−C sample displays two exothermic peaks at around 415 and 604 K, implying the presence of thermodynamically metastable Co−B with different particle sizes. However, Co−B−X displayed only one exothermic peak at 742 K (Figure 4b) higher by at least 138 K than that for Co−B−C. Clearly, the enhanced thermal

Figure 2. TEM image (a) and the corresponding size distribution histogram (b) of Co−B−X. The insert is the high-magnification TEM image of a single nanosphere in part a.

Table 1. Structural Properties of the As-Prepared Catalysts

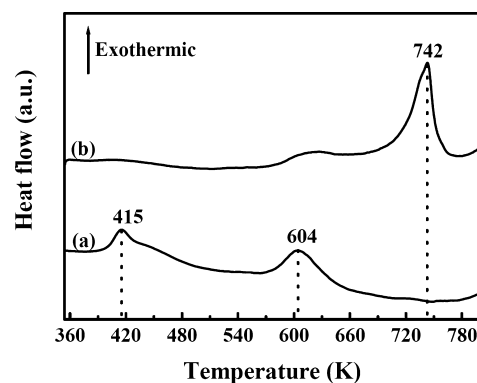| catalyst	composition (atom %)	S_{Co} (m^2 g^{-1})
Co−B−C	Co$_{75}$B$_{25}$	15.3
Co−B−X	Co$_{59}$B$_{41}$	21.9
crystallized Co−B−X[a]	Co$_{59}$B$_{41}$	12.8

[a]Obtained by treating the Co−B−X amorphous alloy at 673 K for 2 h in N$_2$.
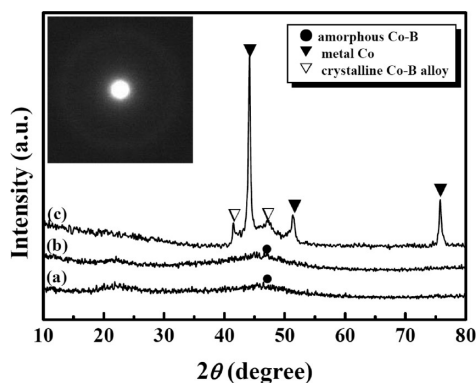
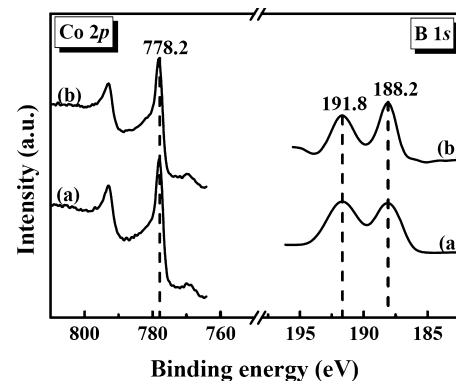**Figure 3.** XRD patterns of (a) the fresh Co−B−C, (b) the fresh Co−B−X, and (c) the Co−B−X sample after being treated at 673 K for 2 h in N$_2$ flow. The insert is the SAED image of the fresh Co−B−X sample.

Figure 4. DSC curves of (a) Co−B−C and (b) Co−B−X catalysts.

Figure 5. XP spectra of (a) Co−B−C and (b) Co−B−X catalysts.

stability against crystallization is first related to the increased B content in Co−B alloys.[19] On the other hand, the uniform particle size may inhibit the particle migration and agglomeration, a key step in the crystallization process resulting from the presence of very tiny particles.[22]

The XPS spectra (Figure 5) reveal that for all Co species in either Co−B−C or Co−B−X, the core level of Co 2p$_{3/2}$ was at 778.2 eV, indicating that all Co atoms were present in the metallic state.[23] But the B species were present in both the elemental B and the oxidized B, with B 1s BE values of around 188.2 and 191.8 eV. The B 1s BE of the elemental B in Co−B−X exceeded that of pure B (187.1 eV) by 1.1 eV,[24] further indicating that the elemental B is alloyed with the metallic Co.

In alloys, partial electrons may be transferred from B to Co, as has been detected in a Co−B−C sample[17] and demonstrated by a theoretical calculation based on the Co$_m$B$_2$ (m = 1−4) cluster models using density functional theory.[25]

The failure in observing the BE shift of the metallic Co can be understood by considering its relatively greater atomic weight compared with the B atom.[24] Thus, considering the results from XRD, SAED, DSC, and XPS, one can conclude that Co−B amorphous alloy was formed through the present

method. According to the calculation based on XPS peak areas, the surface molar ratio of the alloying B to the metallic Co in Co−B−X was 32/68, higher than that in Co−B−C (28/72), implying that Co−B−X was surface-enriched with the alloying B.[19]

Formation Process. The synthesis of the Co−B amorphous alloy through the modified chemical reduction is designed on the basis of the redox reactions as follows:

$$BH_4^- + 2[CoX_4]^{2-} + 2H_2O$$
$$\rightarrow 2Co \downarrow + BO_2^- + 4H^+ + 2H_2 \uparrow + 8X^- \qquad (R1)$$

$$BH_4^- + H_2O \rightarrow B \downarrow + OH^- + 2.5H_2\uparrow \qquad (R2)$$
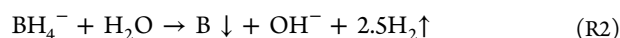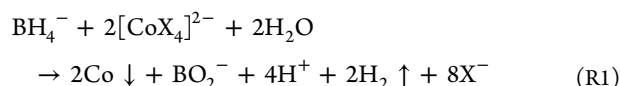
First, KCl and Bu$_4$PBr in water may be dissociated and provide Cl$^-$ and Br$^-$ ions. These halide anions can coordinate with Co^{2+} to form [CoX$_4$]$^{2-}$. The coordination of X$^-$ to Co^{2+} was evidenced by the distinct red shifts of the UV/vis absorption (Supporting Information Figure S1). The absorbance of a CoCl$_2$ solution peaked at around 206 nm. After addition of KCl into the CoCl$_2$ solution, the absorbance peak shifted to 212 nm. When mixed with Bu$_4$PBr solution, a broad absorption peak with a large red shift (219 nm) was observed, which is ascribed to the replacement of the Cl$^-$ ligand by Br$^-$, which has a weaker ligand field and leads to a smaller splitting of the Co^{II} d orbitals.
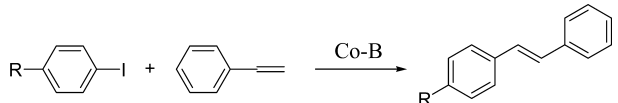
The second step was the reduction of these [CoX$_4$]$^{2-}$ ions by BH$_4^-$. Addition of BH$_4^-$ resulted in chemical reduction of [CoX$_4$]$^{2-}$ ions into Co−B clusters through R$_1$ and R$_2$. The chelating of X$^-$ to Co^{2+} could ensure the reaction between [CoX$_4$]$^{2-}$ and BH$_4^-$ occurred in a homogeneous and smooth manner. In addition, because the ζ-potential of Co−B had been experimentally determined as negative (−18 mV), Bu$_4$P$^+$ could surround the formed Co−B clusters as a result of electrostatic interactions and prevent them from aggregating. The slow reduction process could be further demonstrated by the observation of a crack channel for Co−B−X (inset in Figure 2a). The formation of crack channels might be relative to the hydrogen released during the reduction of [CoX$_4$]$^{2-}$ with BH$_4^-$. Because of the slow reduction rate, the growth of Co−B was around the hydrogen flow and eventually evolves into nanospheres with crack channels.

Both KCl and Bu$_4$PBr played a key role in fabricating monodisperse and uniformly spherical Co−B nanoparticles. Because the coordination of Br$^-$ with Co^{2+} is not strong enough to induce the reaction between [CoBr$_4$]$^{2-}$ and BH$_4^-$ to occurr in a smooth manner, the strongly exothermic reaction led to the formation of irregular Co−B particles in the absence of KCl while keeping other experimental conditions the same as the typical preparation (Supporting Information Figure S2). When Bu$_4$PBr was absent and other experimental conditions were the same as those of the typical synthesis, only broadly dispersed spherical Co−B particles were obtained (Supporting Information Figure S3). Obviously, because of the absence of the stabilizing effect from Bu$_4$P$^+$ ions, a portion of the formed Co−B clusters agglomerated and resulted in the formation of broadly dispersed spherical Co−B particles. These observations implied that the synergistic effect of KCl and Bu$_4$PBr was essential for the formation of monodisperse and uniformly spherical Co−B nanoparticles, which allowed the reduction reaction to take place in a homogeneous and smooth manner and prevented the formed Co−B nanoparticles from agglomerating.

Catalytic Performances. Heck-Type Carbon−Carbon Coupling Reactions. The as-synthesized Co−B amorphous alloy was subjected to Heck-type coupling reactions between an aryl iodide and a terminal alkene, one of the most important reactions for the formation of C−C bonds in organic synthesis.[26] The Heck olefination of iodobenzene has been performed under ligand-free conditions in a mixed solution (DMF/water = 1/1) as solvent, using K$_2$CO$_3$ as the base and a molar ratio of iodobenzene/Co of 50 (Table 2). An excess of

**Table 2. Co−B-Catalyzed Heck-Type Coupling Reaction[a]**

entry	catalyst	R	time (h)	conversion (%)	selectivity (%)
1	Co−B−X	H−	12	98	93
2	Co−B−C	H−	24	99	92
3	Co−B−X	NO$_2$−	12	100	92
4	Co−B−X	CH$_3$−	12	95	90
5	Co−B−X	CH$_3$O−	12	96	92

[a]Reaction conditions: a catalyst containing 5.9 mg Co, aryl iodide (5.0 mmol), pheneylethene (6.0 mmol), K$_2$CO$_3$ (7.5 mmol), water/DMF (5 mL/5 mL), T = 393 K.

styrene with respect to iodobenzene (molar ratio = 1.2) to diminish the formation of a 2-fold coupling byproduct was used. Preliminary studies revealed that oxidized cobalt species could not catalyze such Heck-type coupling reactions under the present conditions, indicating metallic Co was the active site.

To make sure that the Heck coupling reaction carried out on the Co−B amorphous alloy was truly heterogeneous, the reaction between iodobenzene and styrene was allowed to occur until 60% of conversion (Supporting Information Figure S4a), then the solid was filtered out, and the mother solution was allowed to react for another 15 h. No significant change in the conversion of iodobenzene was observed, which confirmed that this reaction really proceeded on the surface of the Co−B nanoparticles because the catalysis by the Co species leached in the solution could be ruled out.

The reaction profiles (Figure 6) reveal that Co−B−X was selective to stilbene (more than 93% throughout the reaction
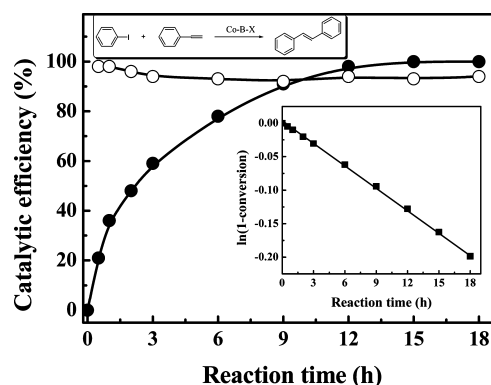
Figure 6. Dependency of the iodobenzene conversion (●) and the diphenylethene selectivity (○) on reaction time over Co−B−X. Inset is the corresponding time−ln(1 − conversion) curve. Reaction conditions are given in Table 2.

process). The obtained ln(1 − conversion) increased almost linearly with the reaction time (inset in Figure 6), indicating the present reaction was first-order with respect to iodobenzene. From the reaction time needed to convert iodobenzene completely, one can see that Co−B−X (entry 1 in Table 2) delivered activity up to 2 times as great as that associated with Co−B−C (entry 2 in Table 2). Clearly, the higher reactivity may be first attributed to the larger number of Co active sites (see S_{Co} in Table 1). However, the S_{Co} of Co−B−X was only 1.4 times that of Co−B−C. Thus, we can argue that Co−B−X possessed enhanced intrinsic reactivity compared with Co−B−C. As identified by the XPS results, Co−B−X had a higher B content than Co−B−C. As a consequence, the Co in Co−B−X was more electron-enriched than Co−B−C,[27] which would allow a more favorable oxidative addition of the metallic Co to the carbon−halogen bond[28] and, therefore, obtain more efficient catalyst. In comparison with the reported metallic Co catalyst, including Co/Al$_2$O$_3$[29] and flower-like Co nanostructure,[30] Co−B−X showed a much higher yield for Heck coupling reactions.

Meanwhile, considering the reaction temperature in our experiments was lower (393 K) than those reported (423[29] and 413 K[30]), Co−B−X obviously was more active than the metallic Co catalysts reported previously. It is worth noting that a significant loss in activity (24%) was observed for Co−B−X in the second recycling experiment, although it has been reported that the use of metallic Co as a catalyst for Heck-type coupling reactions allowed successive batch operations for six[30] and three repeated reactions.[31] The observation of the increase in particle size of the recycled Co−B−X after the second cycle (Figure 7) strongly indicates that the aggregation and
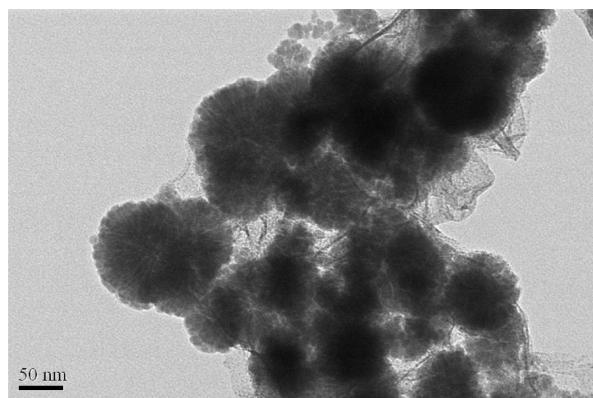
Figure 7. TEM image of the recycled Co−B−X after the second cycle for the Heck-type coupling reaction between iodobenzene and styrene. The reaction conditions are given in Table 2.

precipitation of inactive Co species that occurred during the reaction resulted in a decrease in catalytic activity. Similar deactivation was also observed over Co/Al$_2$O$_3$.[29] Co−B−X was also an active catalyst for the Heck-type coupling reaction of various aryl iodides and styrene. The reactions of iodobenzene with electron-withdrawing or electron-donating groups did not show obvious differences (entries 1, 3−5 in Table 2). This means that the reaction is relatively insensitive to the electronic characteristics of the substituents under the present reaction conditions. In addition, Co−B−X was also active for the Heck coupling reaction between bromobenzene and styrene, although a long reaction time is needed to catalyze this reaction (19 h, 88% conversion, 94% selectivity).

Hydrogenation of Butyraldehyde to *n*-Butanol. Liquid-phase butyraldehyde hydrogenation to *n*-butanol was also used for evaluating the performances of the as-prepared catalyst. Likewise, the hydrogenation of butyraldehyde was confirmed to proceed on the surface of the Co−B nanoparticles using the above-mentioned filtration method (Supporting Information Figure S4b). All the Co-based catalysts displayed nearly 100% selectivity toward *n*-butanol. Figure 8 shows the concentration
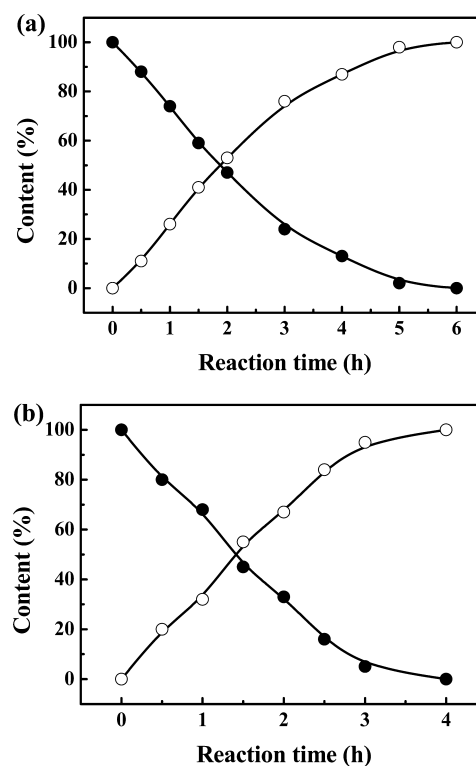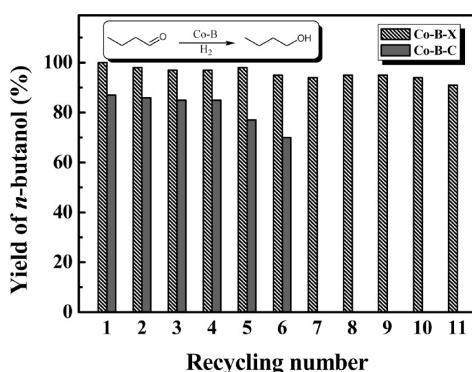

Figure 8. Reaction profiles of butyraldehyde (●) hydrogenation to *n*-butanol (○) over (a) Co−B−C and (b) Co−B−X. Reaction conditions: Catalyst containing 0.3 g Co, 4 mL of butyraldehyde, 45 mL of EtOH, T = 373 K, P_{H_2} = 1.0 MPa, stirring rate = 800 rpm.

change of both the reactant and the product with the reaction time during butyraldehyde hydrogenation over Co−B−C and Co−B−X. As shown in Figure 8, the butyraldehyde conversion increased almost linearly with the reaction time over both Co−B amorphous alloy catalysts, implying that the butyraldehyde hydrogenation was zero-order with respect to butyraldehyde concentration. A significant deviation from the straight line was observed when the butyraldehyde conversion was more than 75%, possibly due to the extremely low butyraldehyde concentration. It is also significant to note that Co−B−X displays enhanced activity compared with Co−B−C, corresponding to a shorter time for achieving the complete conversion of butyraldehyde.

On the basis of reaction rates at conversions between 0 and 10% for the hydrogenation of butyraldehyde, the turnover frequency (TOF) of catalysts was calculated and revealed the intrinsic activity was changed in the following sequence: Co−B−X (0.030 s^{-1}) > Co−B−C (0.021 s^{-1}). As a consequence, the superior activity over Co−B−X to Co−B−C may be attributed to both the larger metallic area (see S_{Co} values) and the enhanced intrinsic activity (see TOF values). The aforementioned XPS analysis revealed that the Co in Co−B−

X was more electron-enriched than that in Co−B−C, taking into account that Co−B−X was surface B-enriched compared with Co−B−C.[27] Accordingly, the higher electron density on Co active sites might be favorable for the formation of H⁻ species[32] and activating the adsorbed C=O group through an electron back-donation from the $d_{x^2-y^2}$ orbital of Co to the $\pi^*_{C=O}$ antibonding orbital of the C=O group,[33] leading to the enhanced TOF. This could be supported by the fact that an abrupt decrease in TOF (0.016 s^{-1}) was observed for the Co−B−X treated at 673 K for 2 h in N$_2$ flow, which was mainly due to the crystallization and decomposition of the Co−B amorphous alloy.

Figure 9 shows the recycling tests using Co−B−X and Co−B−C catalysts. A significant loss in activity (20%) was observed

Figure 9. Recycling tests of Co−B−X and Co−B−C for butyraldehyde hydrogenation. Reaction conditions: Catalyst containing 0.3 g Co, 4 mL of butyraldehyde, 45 mL of EtOH, T = 373 K, P_{H_2} = 1.0 MPa, stirring rate = 800 rpm, t = 4 h.

for Co−B−C after six recycles, whereas Co−B−X could be used repetitively 11 times with a slight loss of activity (8%). ICP analysis reveals that no leaching of the Co species could be detected for Co−B−X and Co−B−C catalysts during repetitive uses, implying that both catalysts were stable against the chelating effect of the reactant and product. Apparently, partial crystallization occurred for the spent Co−B−C catalyst (Supporting Information Figure S5), which was responsible for its deactivation. Co−B−X exhibited much improved durability in comparison with Co−B−C because of its higher surface B content and its uniform particle size and, therefore, its better thermal stability,[19] as confirmed by the aforementioned DSC analysis (Figure 4).

CONCLUSIONS

In summary, our experimental results have indicated a simple route for the preparation of uniform Co−B amorphous alloy nanoparticles through a chemical reduction method by using [CoX$_4$]$^-$ ions as cobalt sources. The Co−B sample thus produced possesses a higher surface B content and uniform particle size, which had been shown to have a positive influence on the catalytic activity in the Heck-type carbon−carbon coupling reactions and the hydrogenation of butyraldehyde to n-butanol. Moreover, these uniform nanoparticles with higher surface B content exhibit superior durability when compared with the conventional Co−B amorphous alloy during the hydrogenation of butyraldehyde owing to the improved thermal stability. Our findings demonstrate the advantages of the present method, making it possible to prepare uniform and stable amorphous alloy catalysts, giving new levels of control over the structures and catalytic performances.

ASSOCIATED CONTENT

Ⓢ Supporting Information
UV/vis spectra of aqueous solutions of CoCl$_2$, CoCl$_2$ + KCl, and CoCl$_2$ + KCl + Bu$_4$PBr; TEM images of Co−B synthesized by the similar conditions used to synthesize Co−B−X but without KCl or without Bu$_4$PBr. Residual activity after filtration for Heck coupling reaction and butyraldehyde hydrogenation. XRD pattern of Co−B−C after six consecutive runs for butyraldehyde hydrogenation. ^{1}H NMR and ^{13}C NMR for (E)-1,2-diphenylethylene, (E)-4-nitrostilbene, (E)-4-methylstilbene, and (E)-4-methoxystilbene. This information is available free of charge via the Internet at http://pubs.acs.org.

AUTHOR INFORMATION

Corresponding Author
*Phone: +86-21-64322272. Fax: +86-21-64322272. E-mail: lihui@shnu.edu.cn.

Notes
The authors declare no competing financial interest.

ACKNOWLEDGMENTS

REFERENCES

(1) Klement, K.; Willens, R. H.; Duwez, P. Nature 1960, 187, 869.
(2) Rinaldi, A.; Correa-Duarte, M. A.; Salgueirino-Maceira, V.; Licoccia, S.; Traversa, E.; Dávila-Ibáñez, A. B.; Peralta, P.; Sieradzki, K. Acta Mater. 2010, 58, 6474.
(3) Rinaldi, A.; Licoccia, S.; Traversa, E.; Sieradzki, K.; Peralta, P.; Dávila-Ibáñez, A. B.; Correa-Duarte, M. A.; Salgueirino, V. J. Phys. Chem. C 2010, 114, 13451.
(4) Dávila-Ibáñez, A. B.; Legido-Soto, J. L.; Rivas, J.; Salgueirino, V. Phys. Chem. Chem. Phys. 2011, 13, 20146.
(5) Van Wonterghem, J.; Mørup, S.; Koch, C. J. W.; Charles, S. W.; Well, S. Nature 1986, 322, 622.
(6) Molnar, A.; Smith, G. V.; Bartok, M. Adv. Catal. 1989, 36, 329.
(7) Baiker, A. Faraday Discuss. Chem. Soc. 1989, 87, 239.
(8) Chen, Y. Catal. Today 1998, 44, 3.
(9) Deng, J. F.; Li, H. X.; Wang, W. J. Catal. Today 1999, 51, 113.
(10) Li, H. X.; Li, H.; Zhang, J.; Dai, W. L.; Qiao, M. H. J. Catal. 2007, 246, 301.
(11) Chiang, S. J.; Liaw, B. J.; Chen, Y. Z. Appl. Catal., A 2007, 319, 144.
(12) Li, H.; Liu, J.; Xie, S. H.; Qiao, M. H.; Dai, W. L.; Li, H. X. J. Catal. 2008, 259, 104.
(13) Li, H.; Zhang, J.; Li, H. X. Catal. Commun. 2007, 8, 2212.
(14) Yasuda, M.; Hayashi, K.; Katoh, Y.; Shibata, I.; Baba, A. J. Am. Chem. Soc. 1998, 120, 715.
(15) Yasuda, M.; Chiba, K.; Baba, A. J. Am. Chem. Soc. 2000, 122, 7549.
(16) Yasuda, M.; Chiba, K.; Ohigashi, N.; Katoh, Y.; Baba, A. J. Am. Chem. Soc. 2003, 125, 7291.
(17) Li, H. X.; Wu, Y. D.; Luo, H. S.; Wang, M. H.; Xu, Y. P. J. Catal. 2003, 214, 15.
(18) Scholten, J. J. F.; Pijers, A. P.; Hustings, A. M. L. Catal. Rev.: Sci. Eng. 1985, 27, 151.
(19) Li, H. X.; Li, H.; Dai, W. L.; Qiao, M. H. Appl. Catal., A 2003, 238, 119.

(20) Yokoyama, A.; Komiyama, H.; Inoue, H.; Masumoto, T.; Kimura, H. M. *J. Catal.* **1981**, *68*, 355.

(21) Martens, K. S.; Parton, J. A.; Vercruysse, R.; Jacobs, K.; Maier, P. A. *Catal. Lett.* **1996**, *38*, 209.

(22) Li, H. X.; Wang, W. J.; Li, H.; Deng, J. F. *J. Catal.* **2000**, *194*, 211.

(23) Mclntyre, N. S.; Cook, M. G. *Anal. Chem.* **1975**, *47*, 2208.

(24) Li, H.; Li, H. X.; Dai, W. L.; Wang, W. J.; Fang, Z. G.; Deng, J. F. *Appl. Surf. Sci.* **1999**, *152*, 25.

(25) Fang, Z. G.; Shen, B. R.; Fan, K. N. *Chin. J. Chem. Phys.* **2002**, *15*, 17.

(26) Heck, R. F. *Acc. Chem. Res.* **1979**, *12*, 146.

(27) Shen, B. R.; Wei, S. Q.; Fan, K. N.; Deng, J. F. *Appl. Phys. A: Mater. Sci. Process.* **1997**, *65*, 295.

(28) Consorti, C. S.; Flores, F. R.; Dupont, J. *J. Am. Chem. Soc.* **2005**, *127*, 12054.

(29) Iyer, S.; Thakur, V. V. *J. Mol. Catal. A* **2000**, *157*, 275.

(30) Qi, H.; Zhang, W.; Wang, X.; Li, H.; Chen, J.; Peng, K.; Shao, M. *Catal. Commun.* **2009**, *10*, 1178.

(31) Zhou, P.; Li, Y.; Sun, P.; Zhou, J.; Bao, J. *Chem. Commun.* **2007**, 1418.

(32) Noller, H.; Lin, W. M. *J. Catal.* **1984**, *85*, 25.

(33) Boellaard, E.; Vreeburg, R. J.; Gijzeman, O. L. J.; Geus, J. W. *J. Mol. Catal.* **1994**, *92*, 299.